Hindawi
Geofluids
Volume 2021, Article ID 5550620, 13 pages
https://doi.org/10.1155/2021/5550620

Research Article

Simulation Study on Image Characteristics of Typical GPR Targets in Water Conservancy Projects

Jie Cao,[1] **Baoyuan Yuan**,[1] **and Yun Bai**[2]

[1]*School of Earth Sciences and Engineering, Hohai University, Nanjing 211100, China*
[2]*Qinghai Province Water Conservancy and Hydropower Survey Design & Research Institute, Xining 810001, China*

Correspondence should be addressed to Jie Cao; 130211030001@hhu.edu.cn

Received 6 January 2021; Revised 18 January 2021; Accepted 29 January 2021; Published 17 March 2021

Academic Editor: Feng Xiong

With the development of the global economy, the deep leakage of reservoirs is still a serious threat to the foundation construction of key water conservancy projects such as dam foundations and bridges. Ground penetrating radar (GPR) is an effective underground imaging and detection technology. In this paper, the Groundvue series of ground penetrating radars is introduced in Britain using the 948 project fund of the Ministry of Water Resources. It is a radar with the lowest frequency in the world at present, improving detection depths and helping to ensure the reliability of a reservoir dam's foundation. Through a large number of field tests, simulation experiments, FDTD numerical simulations, and practical engineering applications, this paper summarizes the reservoir leakage analysis method based on the Groundvue radar. The successful application at the Nanmenxia Reservoir shows that this method can effectively detect the location and path of reservoir leakage and provide technical support for the design and construction of a reservoir reinforcement project.

1. Introduction

Ground penetrating radar (GPR) is a nondestructive technique that uses electromagnetic (EM) waves to image the near subsurface. It has been proven effective and efficient in detecting change in properties. GPR technology has important applications in archaeology [1–4], architecture [5], railways [6], highways [7], water conservancy [8], electric power [9], mining [10, 11], aviation [12, 13], and other fields, and it is also one of the important methods of reservoir leakage detection [14–16]. Although GPR is widely used in the application of reservoir leakage detection, increasing the detection depth, improving the detection accuracy, and improving the interpretation level of data have always been the direction that researchers strive to improve.

The Qinghai Province Water Conservancy and Hydropower Survey Design Institute in collaboration with Hohai University applied for the introduction of the globally advanced technology of the water resources project "geological radar technology introduction and application in Nanmenxia Reservoir and consolidate". With the use of the project funds, the geological radar detection system was introduced. Through a lot of field tests, simulation tests, numerical simulation analysis, and practical engineering applications, we built the system of reservoir deep leakage test and analysis based on the Groundvue radar to improve the reservoir leakage detection depth and the reliability of the geological radar method.

2. Preparatory Work

Among the GV series of radars, the GV6 GPR antenna has a frequency range of 5 MHz-30 MHz and has a center frequency of 15 MHz, which is the radar with the lowest frequency in the world at present. Its detection depth can reach 200 meters underground. This series of radar antennas are divided into shielded and unshielded types, as shown in Figure 1, and the main performance parameters are shown in Table 1. Because of different antenna frequencies, the effective detection depths and detection accuracies of GPR are quite different. Generally speaking, the higher the frequency, the smaller the detection depth, but with a smaller detection resolution and higher accuracy. The antenna detection depth of a 4 GHz antenna is only 0.5 m, but the

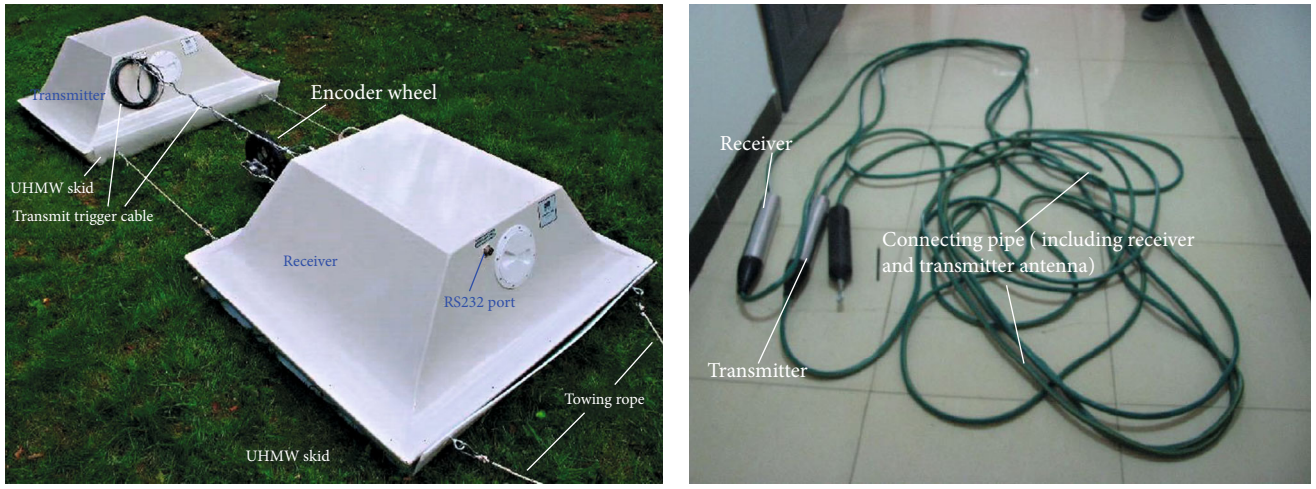

(a) (b)

Figure 1: GPR antenna for Groundvue 2 (shielded (a)) and Groundvue 6 (unshielded (b)).

Table 1: Main performance parameters of the GV series of geological radars.

Types	Depth	Resolution	Antenna frequency
Groundvue 1, 1U	5 m	>5 cm	400 MHz
Groundvue 2	22 m	>0.5 m	50 MHz
Groundvue 3	2 m (50 MHz)	1 cm, 5 cm, 10 cm	4 GHz, 1.5 GHz, 1 GHz, 400 MHz, 250 MHz
Groundvue 4	1 m	0.5 cm	1 GHz
Groundvue 5	0.5 m	1 mm	4 GHz, 6 GHz
Groundvue 6, 6C	200 m, 70 m	2.5 m, 1 m	15 MHz, 40 MHz

resolution can reach 1 mm. The antenna detection depth of a 400 MHz antenna is 5 m, and the resolution is 5 cm. The detection depth of a 15 MHz antenna is 70 m, but the resolution is only 1 m. Thus, the smaller the frequency, the deeper the detection depth, but with the worse resolution. At the same time, shallow multiple reflections may form the illusion of the interface, and it needs to be discriminating when the data is interpreted. It is an important work to detect the image information effectively.

To discriminate between a shallow region, a middle interface or target, or multiple reflections of the formation of the illusion, we can use shallow-, middle-, and high-precision testing for a more accurate determination of shallow central goals and objectives to improve the basis for deep target discrimination. According to the above analysis, the deep-level test analysis method can be used to test a deep target, which is to firstly use the high-frequency antenna to test the shallow region and analyze the section model of the shallow part. In the middle region, the central section model was analyzed, the analysis results of the midsection were used to distinguish the middle target objects, and the central section model was established. Finally, a low frequency antenna was used to test the deep region, and the profile model of the deep part was analyzed, the analysis results in the middle of the analysis were used to identify the deep target objects, and the profile model of the deep part was established.

Therefore, the steps of the GPR test and analysis of deep reservoir leakage are as follows:

(1) Collect the relevant engineering geological conditions, carry out the necessary geological surveys, and master the engineering background of the test

(2) Prepare the relevant GV geological radar testing system and other preparatory work for the test according to the engineering background

(3) Collect typical object simulation test data and carry out the necessary typical target simulation test; the numerical simulation data of typical target objects are collected, and the numerical simulation analysis of typical objects is carried out

(4) Using the deep-level test analysis method in combination with the engineering geological conditions, typical target simulations, laboratory tests, and numerical simulation analysis, achievement of the typical target is attained and the GPR test plan is formulated and the field test conducted

(5) According to the on-site test data, the ReflexW software is used for data processing and interpretation, considering the characteristics of image engineering in anticipation of possible targets, and the necessity

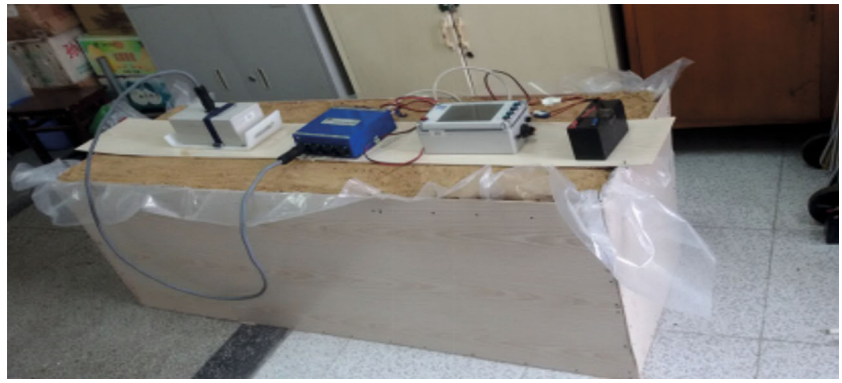

Figure 2: GV3-1 GHz radar test system and laboratory test platform.

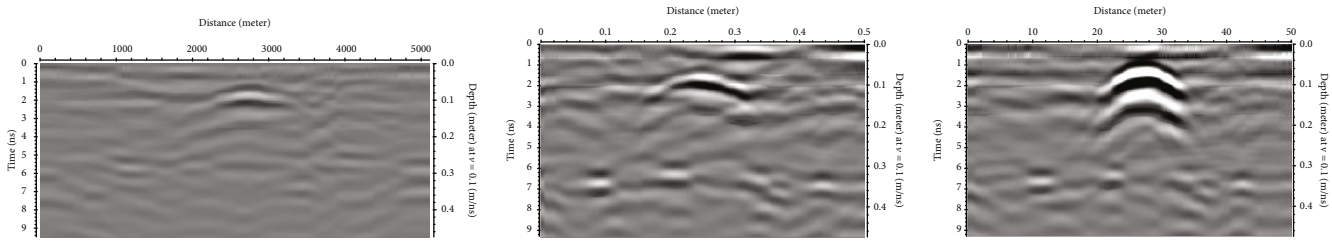

Figure 3: Air pipe (a), plastic pipe (b), and metal pipe (c).

to predict the target model of the simulation and the numerical simulation analysis, using the deep-level analysis method to remove the illusion gradually

(6) Summarize the results of geological radar data interpretation and form geological radar test results

(7) Carry out the necessary drilling work for the geological radar test results and verify the correctness of the results

3. Simulation Test

The simulation test of typical targets and the prediction model is required to establish a simulation test platform. According to the characteristics of GV3-1 GHz GPR, we set up an experimental platform, as shown in Figure 2. The test platform can carry out the simulation test of the typical models, simulate the influence of the main parameters on the geological radar test data, and carry out the simulation test of the target model.

Because there are many reasons for reservoir leakage, the main detection targets are divided into two types according to their shape and size: tubular targets and layered targets. We have carried out a large number of simulation experiments by using the experiment platform, and the following are some typical simulation experiment results.

3.1. Analysis and Research on Radar Test Chart of Tubular Target. For the analysis of tubular objects, we selected materials with different dielectric constants under the same conditions, as shown in Figure 3.

First of all, we can clearly see that the electromagnetic wave reaches the surface of the target and is reflected by the radar test image, thus forming an in-phase axis spectrum image. Although the materials of the three objects are different, the overall shape of the reflex arc is the same. Secondly, with the increase of dielectric constant difference, the intensity of the electromagnetic wave reflection increases.

After observing and studying the gray map of a single target, we did the experiment of two targets in the vertical direction, as shown in Figure 4. The experimental study of vertically placing two pipes is aimed at observing the mutual interference between the upper and lower pipes when the vertical distance changes. From the images, we can see that a group of black and white in-phase axial waves appear when there is only one target, and two groups of black and white in-phase axial waves appear when there are two targets. By comparing the radar gray images, it can be found that with the increase of the number of targets, the electromagnetic wave response becomes stronger, the in-phase axial waves become increasing, and the continuity is enhanced and extends further.

In practical engineering, there are more targets in the longitudinal section, and the situation is more complicated. Based on this, we do the situation of GPR detecting multiple targets, digitize the mutual interference, and get comparable features, which is beneficial to further analyze the features of radar images. If the transmitted and received narrow pulses are ideal, the tubular target should have a conic shape in the gray-scale image of the underground section geological radar. Therefore, the research in this section is to simulate the arc response of the tubular target in the GPR gray map into a

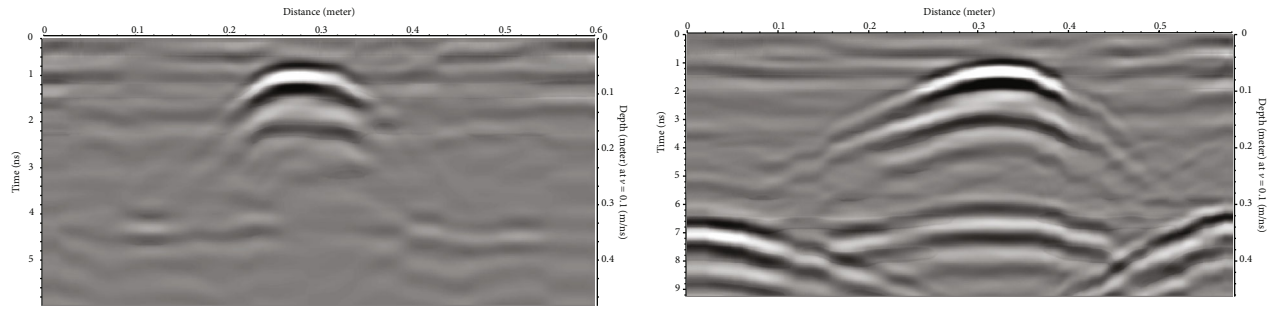

(a) (b)

Figure 4: Single metal pipe (a) and two metal pipes (b).

Figure 5: Spline curves with similar GPR patterns.

quadratic curve, and fit the approximate equation of the quadratic curve which is used to analyze the mutual interference of the GPR detection of multiple tubular targets. The following equation is fitted with Figure 5 as the target.

(1) Import Figure 4(a) into CAD, using fixed-point import, with a scale of 1000. The purpose is to make all imported images have the same scale, analyze under the same conditions, and reduce the impact on the analysis results

(2) In CAD, the spline curve is used to describe the arc reaction of the geological radar gray map of the tubular target, as shown in Figure 5

(3) Deriving control points and fitting points of spline curves, use the instructions in CAD to derive the coordinates of control points and fitting points of the drawn spline curves, which is convenient for the next fitting. See Tables 2 and 3 for the coordinates of control points and fitting points

(4) Origin is used to fit the quadratic curve, and the scatter quadratic spline curve is used to fit. The results are shown in Table 4 and Figure 6

According to the fitting results, the fitting equation is as follows:

$$y = -1.5732 - 0.1508x - 0.0044x^2. \quad (1)$$

Table 2: Coordinates of control points of spline curves.

Control point	x	y	z
1	410.7461	362.6221	0.0000
2	405.2190	359.2446	0.0000
3	432.5675	374.1937	0.0000
4	442.9207	380.6550	0.0000
5	465.3881	386.8810	0.0000
6	485.0444	389.3034	0.0000
7	506.4971	390.0525	0.0000
8	524.2323	384.6467	0.0000
9	545.3661	376.5717	0.0000
10	552.6551	372.9513	0.0000
11	571.8600	358.9635	0.0000
12	569.1632	361.1460	0.0000

Table 3: Coordinates of fitting points of spline curves.

Fitting point	x	y	z
1	410.7461	362.6221	0.0000
2	427.8883	371.7739	0.0000
3	444.1437	380.3352	0.0000
4	463.6503	385.9444	0.0000
5	487.5902	389.1918	0.0000
6	504.7323	389.1918	0.0000
7	525.7167	383.8779	0.0000
8	542.8588	377.3830	0.0000
9	560.5921	367.0504	0.0000
10	569.1632	361.1460	0.0000

Equation fitting is carried out for the reaction arcs of two steel bars in the gray-scale diagram of the GPR experiment in Figure 4(b), and the results are shown in Table 5 and Figure 7.

According to the fitting results, the fitting equation of the arc of the upper reinforcement in Figure 4(b) is as follows:

$$y = -3.5462 - 0.1961x - 0.0058x^2. \quad (2)$$

Table 4: According to the fitting parameters of Figure 5.

Curve	A slope		B1		B2		Statistical correlation coefficient of data
	Value	Standard deviation	Value	Standard deviation	Value	Standard deviation	
Figure 6	-1.5732	0.2507	-0.1508	0.0035	-0.0044	$6.54E-05$	0.9955

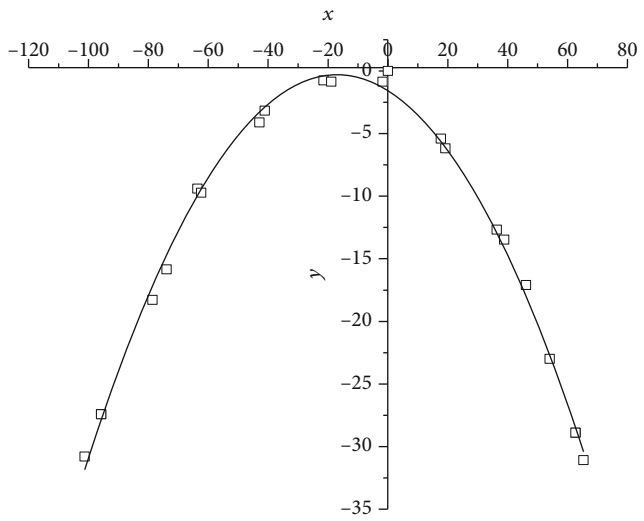

Figure 6: Fitting the equation image according to Figure 5.

The fitting equation of the arc of the lower reinforcement in Figure 4(b) is as follows:

$$y = -4.3448 - 0.2251x - 0.0024x^2. \quad (3)$$

By analyzing the fitting equation, the curvature k of the arc at the highest point can be calculated. The curvature radius of the upper reinforcement is 86 and that of the lower reinforcement is 210 in Figure 4(b). According to the fitting equation in Figure 4(a), the radius of curvature is 112. The results are shown in Table 6.

The analysis of Table 6 shows that when two reinforcing bars are buried vertically and shallowly, the curvature radius 86 of the response radian of the GPR gray map of the upper reinforcing bar is smaller than the curvature radius 112 of the response radian of the GPR gray map when one pipe is buried alone. The variable in the experiment is only that one reinforcing bar is placed under the pipe, so it can be considered that the reinforcing bar buried in the lower layer will affect the one buried in the upper layer, which makes the curvature radius of the response radian of the GPR gray map of the upper reinforcing bar smaller.

When two steel bars are buried vertically and shallowly, the curvature radius 120 of the response radian of the GPR gray map of the lower steel bar becomes larger than the curvature radius 112 of the response radian of the GPR gray map of the single buried pipe. The variable in the experiment is that only one steel bar is placed on the top of the pipe, so it can be considered that the upper buried steel bar will influence the detection of the lower one, which makes the curvature radius of the response radian of the lower steel bar become larger.

This is the guiding significance when using GV series GPR to detect multilayer tubular targets with an up-down relationship in practical engineering.

3.2. Experimental Error Analysis. To compare the error between the actual buried depth and the experimental buried depth, we will list and analyze the experimental data, as shown in Table 7. It can be seen that the absolute error between the actual buried depth of the tubular target and the experimental detection depth in the experiment is less than 1 cm, except for the PVC pipe on the south side of the sandbox with a buried depth of about 30 cm. It shows that GV3 GPR has high detection depth accuracy.

With the increase of buried depth, the absolute error of detection depth gradually increases, which shows that the error of detection depth increases gradually with the depth due to the change of environment. At the same time, the relative error of detection depth is always within 5%, which shows that the detection accuracy of GV3 GPR is stable.

Error analysis is as follows:

(1) Because of the system error of the instrument itself, each set of instruments will have a certain system error due to the calculation method, instrument accuracy, and so on, which needs technical progress to improve

(2) There is an error in the actual buried depth in the experiment, because the actual buried depth in the sample is measured with a ruler, and the minimum scale of the ruler is millimeters, which makes it necessary to evaluate the reading and affects the measurement accuracy

(3) There will be errors in two-way travel time, and the one-way travel time of detecting the tubular target is read by selecting suitable points on the gray-scale map of geological radar, which makes the final one-way travel time error due to human factors in selecting points

(4) Calculation error of electromagnetic wave velocity. In this experiment, the relative dielectric constant method is used to calculate the electromagnetic wave velocity, and the relative dielectric constant of a sand body is an empirical value, so there will be an error in the actual relative dielectric constant, which will affect the calculation of electromagnetic wave velocity. In practical engineering, the method of field measurement of electromagnetic wave velocity should be adopted to be more accurate

Table 5: According to the fitted parameters of Figure 4(b).

Curve	A slope		B1		B2		Statistical correlation coefficient of data
	Value	Standard deviation	Value	Standard deviation	Value	Standard deviation	
Figure 4(b) upper reinforcement	-3.54617	0.52079	-0.19613	0.0077	-0.00579	$1.47E-04$	0.98556
Figure 4(b) lower reinforcement	-4.3448	0.79552	-0.22513	0.00905	-0.00238	$7.76E-05$	0.9803

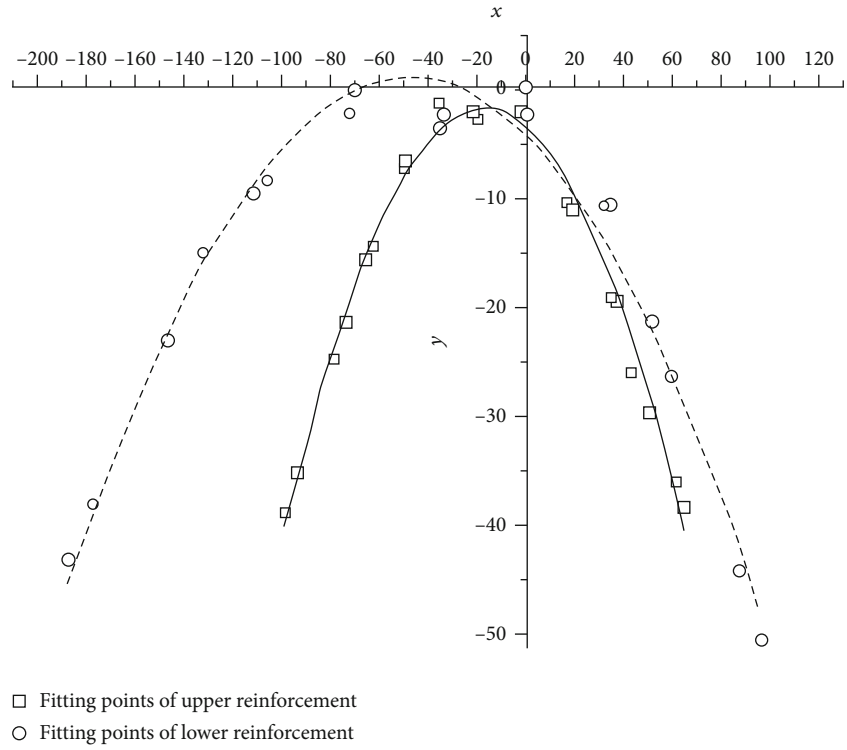

Figure 7: According to the equation image of curve fitting in Figure 4(b).

Table 6: Calculation result of the fitting curve.

Experiment target	Calibre	Depth	Radius of curvature
Single steel bar	3	10	112
Two steel bars(upper)	3	10	86
Two steel bars(lower)	3	20	210

3.3. Analysis and Research on Radar Test Chart of Layered Target. Water is widely distributed in strata and plays an essential role in engineering. It is an essential part in the application of GPR to detect water-bearing structures.

First of all, in the nonaquifer and aquifer simulation experiment scheme, the environmental medium is dry sand, and the target objects are ceramic tiles; the ceramic tiles, with dimensions of 30 cm ∗ 30 cm ∗ 3 cm, are soaked overnight and buried at a depth of 20 cm. The experimental results are shown in Figure 8. Figure 9 shows the detection results of dry and wet sand stratification, in which the upper part is dry sand medium and the lower part is wet sand medium without other objects, and the interface between the two media is 30 cm deep.

Compared with the results in Figure 8, under other conditions being the same, the reflection image of the ceramic tile after soaking in water is much stronger, the amplitude is enhanced, and the diffraction and scattering phenomena inside the ceramic tile are also greatly enhanced. It shows that water will increase the dielectric constant of the target, which has a very obvious detection effect in GPR.

It can be observed from Figure 9 that the electromagnetic properties and structural characteristics of dry sand and wet sand media are different, and the reflection conditions of electromagnetic waves propagating in them are also different. The reflected waves in wet sand are stronger than those in dry sand, and the frequency is relatively high. Because of the different structures and properties of different media, the reflection and absorption ability of electromagnetic waves are different, and the spectral characteristics of reflected waves in GPR detection results are also different, which shows that the spectral characteristics of reflected waves are also the basis for distinguishing different material interfaces when using GPR to detect layered media. According to its

Table 7: Error analysis table of radar detection test for PVC pipes with different depths.

Target parameter	Actual depth (cm)	Two-way travel time (ns)	Detecting depth (cm)	Buried depth error (cm)	Relative error (%)
PVC pipe on the south side with a buried depth of 10 cm	10.5	1.4444	10.833	0.333	3.2
PVC pipe on the north side with a buried depth of 10 cm	10	1.2939	9.704	-0.296	-3.0
PVC pipe on the south side with a buried depth of 20 cm	20	2.5532	19.149	-0.851	-4.3
PVC pipe on the north side with a buried depth of 20 cm	21	2.8535	21.401	0.401	1.9
PVC pipe on the south side with a buried depth of 30 cm	30	4.1451	31.088	1.088	3.6
PVC pipe on the north side with a buried depth of 30 cm	30	4.1095	30.821	0.821	2.7

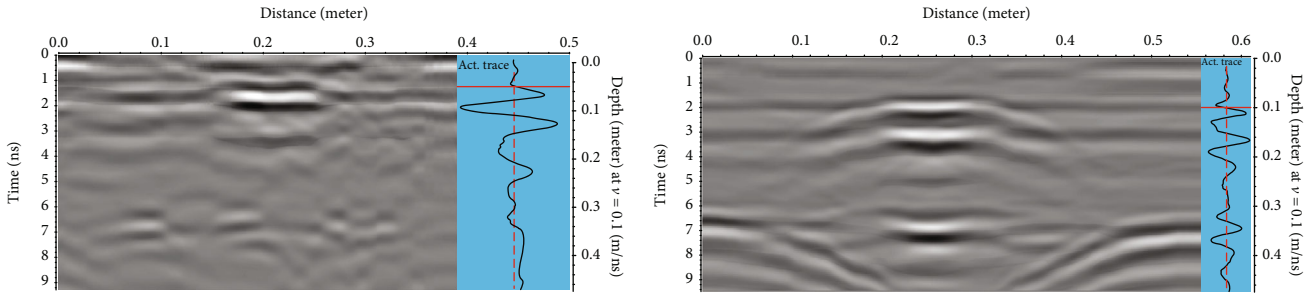

Figure 8: Gray map of radar detection of dry tile (a) and wet tile (b).

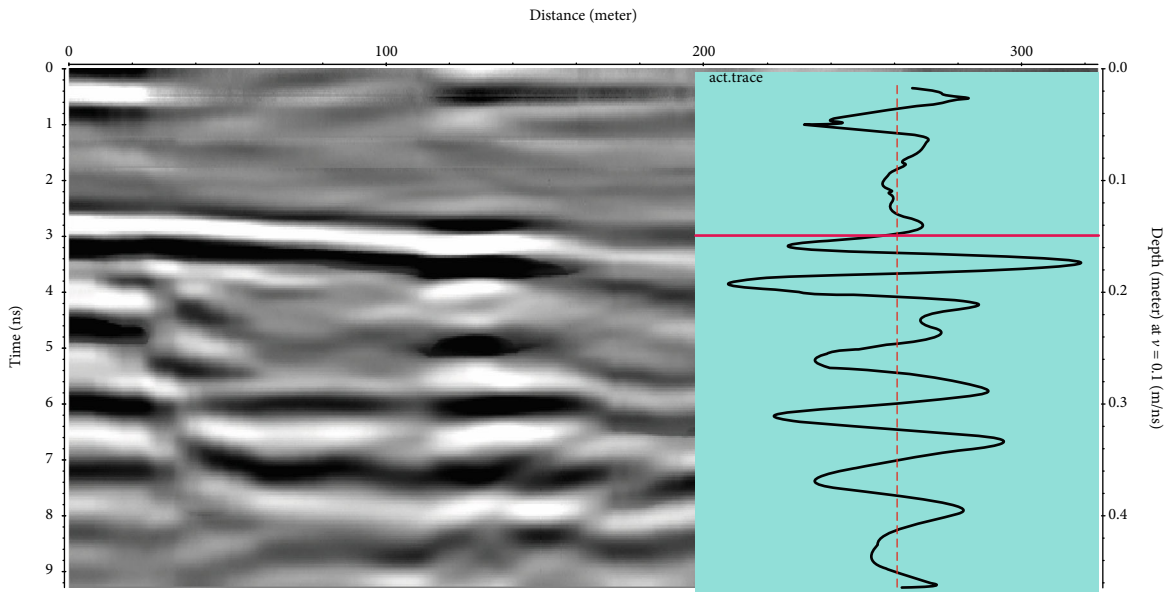

Figure 9: Radar detection gray of dry sand and wet sand stratification.

electromagnetic wave reflection frequency, it can be divided into low frequency, medium frequency, and high frequency. In the medium with a relatively complete and uniform structure, the internal reflection wave is less, and the reflection wave frequency is generally lower, while in the medium with uneven material composition and developed joints and fissures, the reflection wave frequency will clearly increase. The intensity of the reflected wave is mainly related to electromagnetic properties such as the dielectric constant of the medium, which can be divided into strong reflection and weak reflection according to the amplitude of the reflected wave. Generally, the greater the difference of the dielectric constant between the two sides of the reflective layer, the greater the intensity of the reflected wave. In addition, the intensity of the reflected wave received by GPR is also related to the absorption ability of the upper medium to the electromagnetic waves.

The dielectric constant of water is more than 80, so the aquifer is a low-wave velocity layer, which is quite different from other strata above and below. The image characteristics

of an aquifer in GPR detection have a clear interface and a strong reflection. When the electromagnetic wave passes through the upper interface of an aquifer, the reflection coefficient is negative, and the phase of the reflected wave is opposite to that of the incident wave, while when passing through the lower interface, the reflection coefficient is positive, and the phase of the reflected wave is connected with that of the incident wave. When the electromagnetic wave penetrates the aquifer, it will produce regular multiple strong reflections, generate diffraction and scattering phenomena in the water-rich zone, and the energy of the electromagnetic wave will decay rapidly. Because water is unevenly divided in rock fractures, the reflection images of water-bearing rock masses are generally messy and have no obvious in-phase axis. In Quaternary aquifers, the water layer is usually continuously divided, so its image features are continuous layers and relatively uniform waveforms. According to the conclusions obtained from Figures 8 and 9, the amplitude direction and spectrum characteristics of reflected waves are important identification marks of layered media detection by ground penetrating radar. By observing the amplitude direction and spectrum characteristics of the reflected waves, the electromagnetic properties of interfaces and media on both sides can be identified, and thus the detection targets can be determined.

Secondly, the fracture zone is a common geological structure in reservoir leakage, which is usually distributed in a zonal pattern. The integrity of a rock mass is destroyed by geological tectonic movement, which makes its structure and composition become very complex. Figure 10 shows the ground penetrating radar detection results of the simulated fracture zone indoors. The medium is dry sand, and the target is that multiple bags of wet sand with slight differences in water content are closely arranged in a simulated fracture zone with a buried depth of 20 cm. From the experimental results, it can be seen that there is obvious strong reflection, the in-phase axis is discontinuous, the figure is messy, and there is no unified reflection interface.

In the experiment, the target water content difference and gap are still relatively small, but the actual fractured zone has uneven water content, developed joints and cracks, often has weak interlayer appearance, and there are uneven fillers with different electromagnetic properties in the cracks. Combined with the above figure, the geological radar image of the fracture zone is characterized by a series of chaotic strong reflections, discontinuous in-phase axis, significantly enhanced amplitude near the reflecting surface, fine and messy waveform, diffraction and scattering phenomena inside, and fast attenuation of electromagnetic wave energy, etc.

Finally, in the actual project, because of different survey line positions or irregular arrangement of targets, we designed the pipe-shaped target tilt experiment, as shown in Figure 11. It is obvious that the electromagnetic wave reflex arc is similar to the layer, and the arc-shaped reflex arc at both ends appear at the position 10 cm below the sand body surface, which is judged as the starting point for the ground penetrating radar wave to detect the target. According to the image, we can see clearly that the angle of the target is the same as the detected angle. To sum up, the position of the image is consistent with the buried position of the actual target, and it can be confirmed that the image is the geological radar gray map of the target.

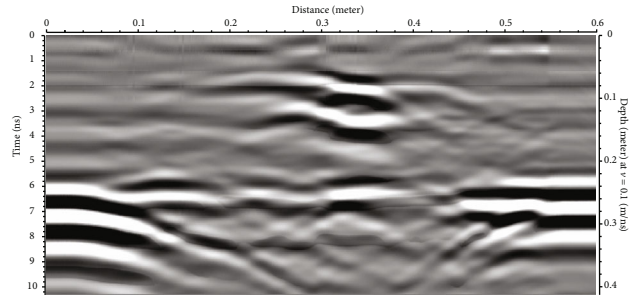

Figure 10: Detection results of a simulated fracture zone.

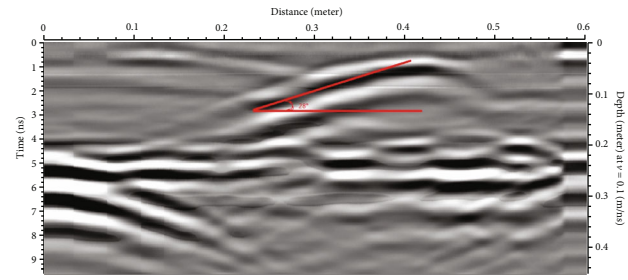

(a)

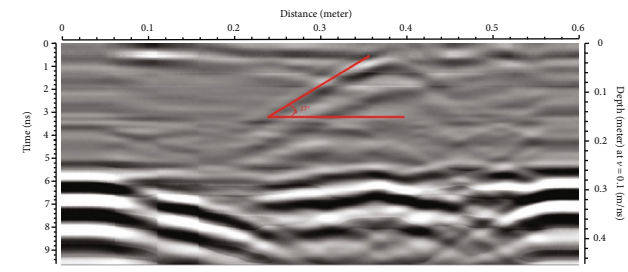

(b)

Figure 11: Gray map of radar detection of tubular target with inclination angles of 30 (a) and 45 (b).

4. Numerical Simulation Analysis

GprMax2D is a numerical simulation software based on the FDTD algorithm and the PML boundary absorption conditions introduced by Dr. Antonis Giannopoulos of the University of Edinburgh School of Electrical Engineering, in 1996. GprMax2D is used for the study of geologic radar imaging. The GprMax2D source code was originally derived from Dr. Antonis Giannopoulos's doctoral dissertation on GPR imaging, which has evolved to version 2.0 after more than a decade of improvement [17]. The main features of the GprMax2D software include a simple command interface, the ability to model the dispersion medium and target objects that can simulate complex shapes, and strong absorption boundary conditions. GprMax2D can be used to simulate the isotropic homogeneous medium, simulate the propagation of electromagnetic waves in the Debye

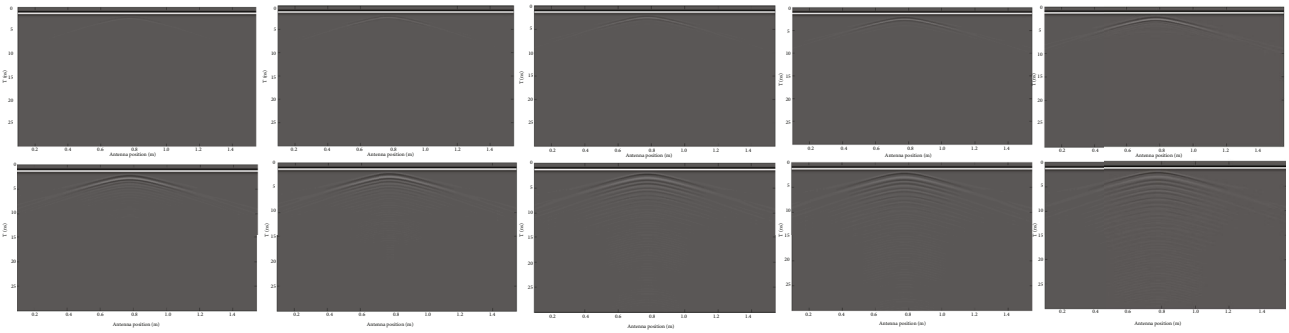

Figure 12: Gray diagram of numerical simulation of a tubular object with change of dielectric constant.

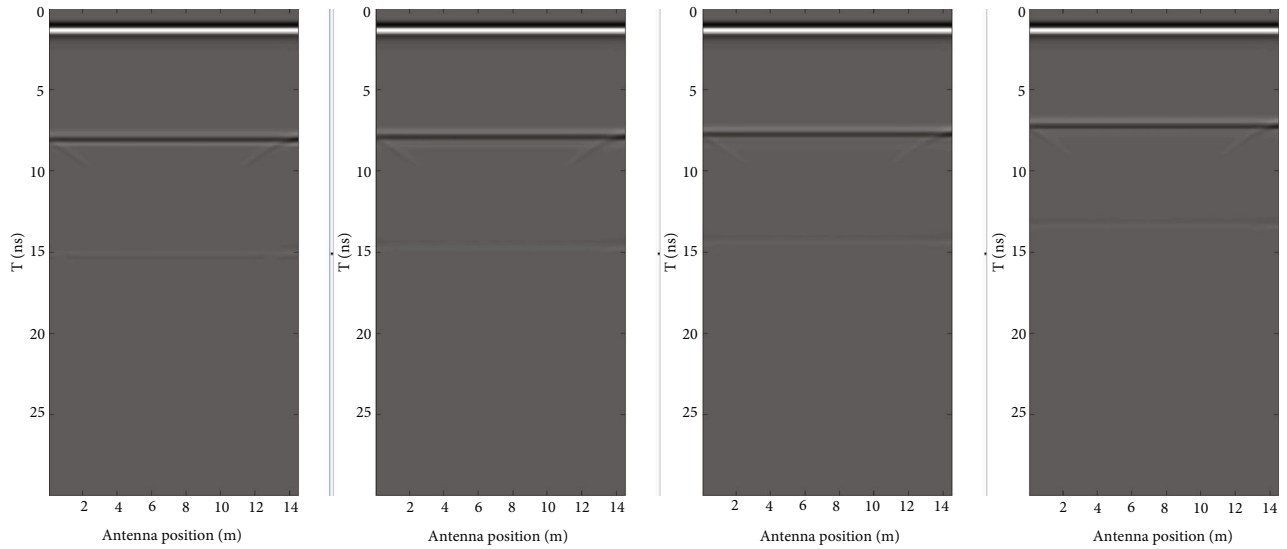

Figure 13: Gray diagram of numerical simulation of a layered object with thickness change.

dispersion medium, and simulate the interaction between electromagnetic waves and targets, to obtain the geological radar echo of the target [17].

To study the regular changes of typical targets detected by ground penetrating radar, we use the GprMaxV2.0 software to carry out numerical simulation experiments. In the model, the simulated environment is relatively uniform dry sand, and the center frequency of the simulated signal is 900 MHz. The simulation results are shown in Figures 12 and 13. From Figure 12, we can see that at first, the image of the tubular object is parabolic. Secondly, as the difference between the dielectric constant of the target object and the simulated environment becomes larger, the identifiability of the image becomes higher and higher, and the image extends farther and farther to both sides. The appearance of the last multiple shows that the dielectric constants of the target and the environment are quite different, similar to aquifers, mineral layers, and so on. The above image features are consistent with the laboratory test results. Combined with Figure 13, we get that when the object is layered, the middle part of the image is a straight line, and both ends are half branches of the parabola. The increase in the thickness of the target can also be recognized in the image. The features of this image also conform with the laboratory test results.

5. Engineering Application

The Nanmenxia Reservoir is a Class III medium-sized project with irrigation as the main project. It was built in 1974 and put into operation in 1982, as shown in Figure 14. Because the reservoir is located in a karst area, the geological conditions are complex, and karst and fissures developed in the dam foundation and dam abutments on both sides, resulting in serious leakage. The reservoir has undergone many antiseepage treatments. However, due to the unclear distribution of karst and fissures, all previous antiseepage treatments have no obvious effect. In this project, the British Groundvue series GPR system is introduced, and through field test and drilling verification, the distribution and path of karst leakage in the Nanmenxia Reservoir have been determined, which provides the basis and guidance for improving the reinforcement effect, giving full play to the social and economic benefits of the reservoir and preventing major disasters. With approval from Ministry of Water Resources, the project was reinforced.

(a) Satellite map of reservoir

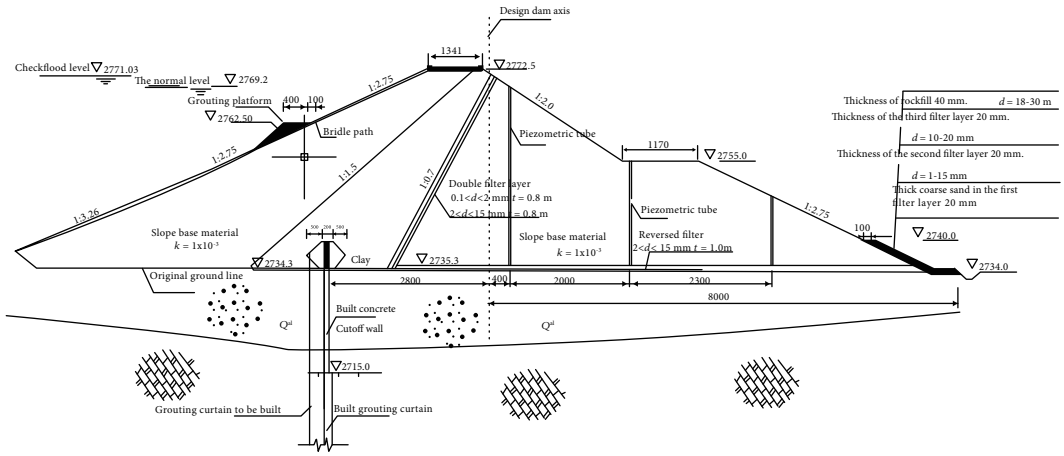

(b) Sectional view of the Nanmenxia Reservoir dam

Figure 14: Satellite map of reservoir (a) and sectional view of the Nanmenxia Reservoir dam (b).

Firstly, according to the engineering characteristics of the Nanmenxia Reservoir, we have carried out a large number of simulation experiments and numerical simulation experiments of typical objects and worked out the test scheme. According to the engineering conditions of the Nanmenxia Reservoir, the GV3-400 MHz antenna was selected to test the shallow part, the GV2-50 MHz antenna was selected to test the middle part, and the GV6-15 MHz antenna was selected to test the deep part. According to the characteristics of the Groundvue series GPR, the detection mode of continuous profile scanning was selected. Different types of radars were used, and because of their different detection depths and precision, the measurement results of radar detection in the same detection section are compared and analyzed, and complement each other. See Figure 15 for the schematic layout of the survey lines. Combined with the actual measurement data, the simulation experiment and numerical simulation analysis of the prejudgment model are carried out, and the effective conclusions related to reservoir reinforcement are obtained, some of which have been well verified by drilling work, as shown in Figure 16(b). The main achievements are as follows:

(1) GPR test analysis was carried out in the grouting adit on the right bank of the reservoir dam, and the test result is shown in Figure 17(a). The results show that

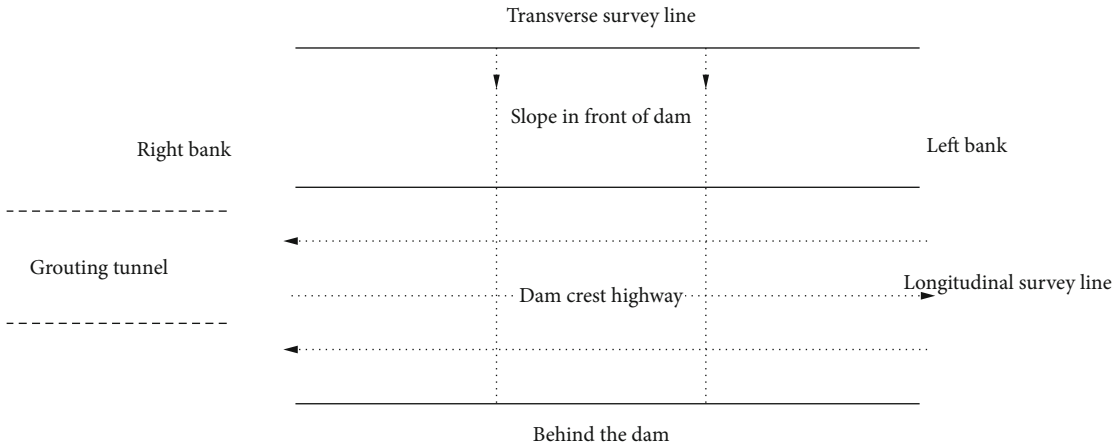

Figure 15: Schematic diagram of ground penetrating radar survey line layout.

(a) (b)

Figure 16: Photo of the groundwater flowing borehole behind the dam (a) and core drilled on site (b).

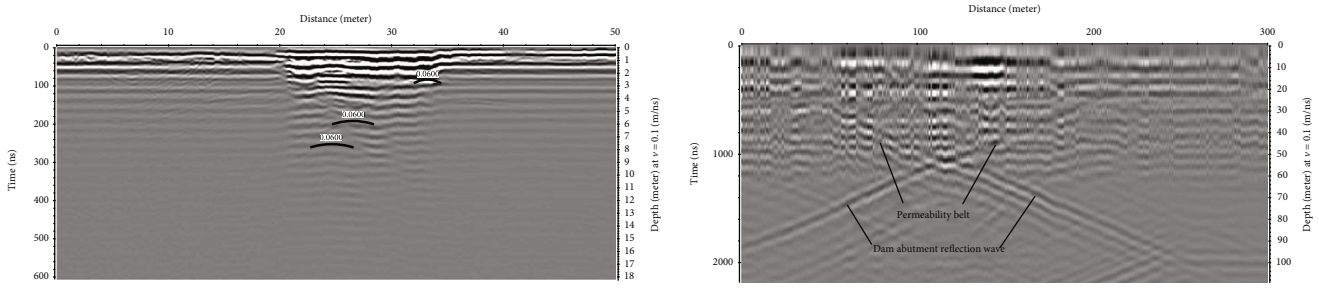

(a) (b)

Figure 17: Gray chart of radar test of grouting adit on the right bank (a) and gray map of ground penetrating radar test for bedrock of dam foundation (b).

there are obvious fracture development zones in the 0 + 450 ~ 0 + 470 m section of the grouting adit on the right bank. We can see that the in-phase axis at the depth of 10 m-35 m is intermittent, and the image waveform is disordered and strongly reflected. Among them, the waveform response from 10 m to 25 m in the image is strong, and this phenomenon continues down to the depth of 9 m. It is speculated that the continuity of strata is not good due to rock mass breakage. Because water may be contained in fractures, the waveform reaction is strong, and multiple strong reflections with certain regularity will occur in the lower strata. The grouting flat tunnel is 20 m from the entrance to the inside and 4 m deep, and it is judged as wet soil according to the speed discrimination. The same situation still appears at 39 m and 3 m depth, but the difference is that the image response is not as strong as the previous one, and it hardly extends to the deep part, which is probably the reason of the less water content. In the range of 21 m and 2 m to 5 m depth, there are many arcs with downward openings, but they do not extend to the

deep part, so it is speculated that the fractures are developed and the water content is less

(2) Through the GPR test at the bottom of the dam slope in the axial direction of the dam, it was found that there was an obviously strong permeability zone in the bedrock under the overburden in the range of about 50 m from 0 + 155 m to 0 + 205 m, as shown in Figure 17(b). Because it is located on the original runoff path, there will inevitably be an infiltration section below the stratum, which contains more water. In addition, GV6 GPR does not have an external metal cover to shield the external interference, which is unfavorable for GPR detection. The figure contains many sharp spikes, which depict noise interference, and the waveform attenuation is severe. It can be seen in the figure that the two intersecting oblique lines are the surface interfaces, and the propagation velocities represented by the two oblique lines are the same, but the phases are opposite. On the radar image, the oblique angles of the two lines are the same, but the oblique directions are opposite. It can still be seen from the observation images that within the range of 0 + 155 ~ 0 + 205 m, which is about 50 m of the dam section, from the surface down to the depth of 60 m, the GPR images have strong signal response and uneven energy distribution, and the intermittent axis in the same direction indicates that the continuity of the stratum is poor, and the waveform reflection in some survey sections is strong, and it shows regular multiple strong reflections to the deep and gradually decays, which should be a water-bearing fracture. Self-spraying drilling on the platform behind the dam also proves that this section has strong water permeability and certain pressure bearing, as shown in Figure 16(a).

6. Conclusion

(1) The reservoir deep leakage detection and analysis system based on the Groundvue geological radar is composed of the Groundvue radar instrument system, the ReflexW interpretation system, simulation tests, numerical simulation analysis, and a step-by-step analytic hierarchy process and drilling verification method, which is an integrated system

(2) The test platform provides conditions for the simulation experiment of the typical targets and the simulation experiment of the prejudgment target model, which is helpful to improve the technical personnel's proficiency level in GPR data analysis and interpretation. The numerical simulation method can provide conditions for the simulation analysis of typical targets and the prediction target model, which is helpful to understand the influence of the change of the main parameters on GPR images

(3) Simulation experiment combined with numerical simulation analysis can eliminate simulation test material parameters in fixed and limited experiments; it can also eliminate the influence of the image which is caused by the numerical simulation image and actual radar image deviation, forming a point-line integrated simulation method

(4) Geological radar detection of the south gate gorge reservoir solved the leakage problem, a problem which had caused trouble to the dam foundation for many years, and fully proving the effectiveness of the reservoir deep leakage detection analysis system based on GPR

Data Availability

The data used to support the findings of this study is included within the article.

Conflicts of Interest

The authors declare that they have no conflicts of interest.

Acknowledgments

This paper relied on the support from the 948 Project Fund of the Ministry of Water Resources. The authors are especially grateful to Professor Yuan Baoyuan for his careful guidance in developing the thesis; to Mr. Baiyun, a senior engineer; and to the laboratory team of Hohai University for their cooperation and help.

References

[1] M. Pinpan, L. Baradello, E. Forte, A. Prizzon, and I. Finetti, "2-D and 3-D processing and interpretation of multi-fold ground penetrating radar data: a case history from an archaeological site," *Journal of Applied Geophysics*, vol. 41, pp. 271–292, 1999.

[2] V. P. Gracia, J. A. Canas, L. G. Pujades et al., "GPR survey to confirm the location of ancient structures under the Valencian Cathedral (Spain)," *Journal of Applied Geophysics*, vol. 43, no. 2-4, pp. 167–174, 2000.

[3] A. P. Annan, *Groud penetrating radar application principles, procedures and applications*, Sensors & Software Inc., 2003.

[4] R. G. Francese, E. Finzi, and G. Morelli, "3-D high-resolution multi-channel radar investigation of a Roman village in Northern Italy," *Journal of Applied Geophysics*, vol. 67, no. 1, pp. 41–51, 2009.

[5] Y. Zhao, J. Chen, and S. Wang, "Application of ground penetrating radar for limestone foundation of high building," *Chinese Journal of Underground Space and Engineering*, vol. 2, no. 4, pp. 700–704, 2006.

[6] Y. Yang, S. He, and F. Qi, "Simulation test of GPR non-contact detection on lining of railway tunnel," *Chinese Journal of Rock Mechanics and Engineering*, vol. 30, no. 9, pp. 1761–1771, 2011.

[7] C. Lu, Z. Qin, and H. Zhu, "Practical methods for detection of concealed cracks in high way pavement using ground penetration radar data," *Chinese Journal Geophys*, vol. 50, no. 5, pp. 1558–1568, 2007.

[8] F. Wu, "Application of GPR in the dam foundation engineering of hydropower station," *Journal of North China Institute of Water Conservancy and Hydroelectric Power*, vol. 33, no. 3, pp. 94–96, 2012.

[9] X. Xie, G. Hong, and G. Tang, "The research on development of GPR antenna and modeling test of cable duct cracks with pipe GPR," *Chinese Journal of Underground Space and Engineering*, vol. 11, no. 2, pp. 756–763, 2015.

[10] W. Yang and S. Deng, "The GPR detection of unknown mining cavities beneath the foundation piles," *Chinese Journal of Engineering Geophysics*, vol. 6, no. 1, pp. 23–27, 2009.

[11] S. Deng, B. Mei, and C. Hu, "Ground penetrating radar detection of underground unknown mining cavities in the open-pit at the Zijinshan Au-Cu deposit," *Mineral Resources and Geology*, vol. 22, no. 3, pp. 255–269, 2008.

[12] H. Liu, "A new method for the investigation of the airborne radar," *Geology in China*, vol. 3, pp. 15–17, 1987.

[13] H. Yang and L. Wang, "Application of aerial side-view radar image," *Remote Sensing Information*, vol. 1, pp. 38–40, 1987.

[14] S. Ge, G. Liang, and Y. Chen, "Application of GPR and high-density resistivity method to leakage detection of dam bodies," *Advances in Science and Technology of Water Resources*, vol. 25, no. 5, pp. 55–57, 2005.

[15] S. Ge, S. Zhang, and Q. Li, "Experimentation and analysis on the application of detecting hollow injury in the sea wall by means of ground penetrating radar," *Progress in Geophysics*, vol. 22, no. 3, pp. 989–993, 2007.

[16] S. Ge, X. Liu, and Y. Zhao, "Application research of detecting technology for seawall hidden defects and grouting effect," *Chinese Journal of Underground Space and Engineering*, vol. 9, no. 1, pp. 42–47, 2013.

[17] A. Giannopoulos, "Modelling ground penetrating radar by GprMax," *Construction and Building Materials*, vol. 19, pp. 755–762, 2005.